Carbon Contamination during Melting Process of Czochralski Silicon Crystal Growth

Liu, Xin
Research Institute for Applied Mechanics, Kyushu University

Gao, Bing
Research Institute for Applied Mechanics, Kyushu University

Nakano, Satoshi
Research Institute for Applied Mechanics, Kyushu University

Kakimoto, Koichi
Research Institute for Applied Mechanics, Kyushu University

https://doi.org/10.15017/1526210

出版情報：九州大学応用力学研究所所報. 147, pp.1-5, 2014-09. Research Institute for Applied Mechanics, Kyushu University
バージョン：
権利関係：

Carbon Contamination during Melting Process of Czochralski Silicon Crystal Growth

Xin LIU[*1], Bing GAO[*1], Satoshi NAKANO[*1] and Koichi KAKIMOTO[*1]

E-mail of corresponding author: *liuxin@riam.kyushu-u.ac.jp*

(Received July 31, 2014)

Abstract

Czochralski (CZ) growth of single silicon (Si) crystals is invariably accompanied by transport of impurities such as carbon (C), oxygen (O) and related compounds produced by reactions at high temperatures. To study the generation and accumulation of C during the melting process, a transient global model was developed including coupled O and C transport. The enthalpy method for phase change problem was introduced to investigate the melting process. Transport phenomena of C, O and related compounds were predicted by considering five chemical reactions in the furnace. The dynamic behavior of impurities was revealed during the melting process of the Si feedstock. It was found that contamination with C is activated once the melting front contacts the argon gas. The results indicate that C accumulated during the melting process. For accurate control of C contamination in CZ-Si crystals, the accumulation of C during the melting stage should be taken into account.

Keywords: *Computer simulation, Impurities, Mass transfer, Czochralski method*

1. Introduction

The Czochralski (CZ) method is the favored technique to produce bulk single crystals for a wide range of electronic and photovoltaic wafers. CZ growth of single silicon (Si) crystals is invariably accompanied by transport of impurities, such as carbon (C), oxygen (O) and related resultants from reactions at high temperature.[1)] Contamination with C can lead to degradation of Si wafers through the formation of C-induced defects.[2)] The concentration of O should also be accurately controlled because it affects the formation of micro-defects in the growing crystal in a complex manner.[3)] Thus, the transport mechanism of impurities and how to control their concentrations in a crystal are important for wafer and device manufacture.

Besides impurities in the feedstock itself, C mainly comes from graphite components in the furnace, while O originates from the dissolution of the quartz crucible. O and C are strongly correlated with gaseous SiO and CO, which are the products of numerous reactions in CZ-Si crystal growth. These reactions are triggered during the heating and melting stages, and occur until crystal growth ceases. An experimental investigation[4)] demonstrated that the concentration of CO in the gas in a furnace increases considerably during the melting process. However, the dynamic behavior of CO generation and C contamination during the melting process has not been reported to date. Therefore, here we investigate the coupled transport of O and C during the melting stage of CZ-Si crystal growth.

Si melt and argon (Ar) gas act as impurity carriers of C, O and related compounds like CO and SiO. To investigate the transport mechanism of C and CO in a CZ-Si furnace, Bornside *et al.*[5)] derived a chemical model of CO and SiO from thermodynamic analysis of their reactions. Based on this chemical model, Gao and coworkers[6)] developed the coupled transport model for SiO and CO in Ar gas and C and O in a Si melt. The coupled impurity transport model was also used in global modeling of the directional solidification (DS) process for multicrystalline Si.[7, 8)] Recently, Vorob'ev *et al.*[9)] reviewed chemical models and impurity transport for global modeling of CZ-Si and DS-Si crystal growth. However, most of these global simulations focused on analysis of steady-state growth of CZ-Si using the quasi-steady-state assumption. Few researchers have addressed the generation and contamination of species during the melting stage in a CZ-Si furnace.

The present study focuses on heat and mass transport during the melting stage of CZ-Si crystal growth. To study the dynamic behavior of impurity transport, a transient global model for the melting process is developed, including the heat and mass transport in Ar gas. The enthalpy method for the convection/diffusion phase change problem is introduced to capture the melting fronts in a feedstock in a quartz crucible. Five chemical reactions are included at the interface

*1 Research Institute for Applied Mechanics, Kyushu Univ.

of impurity generation and conversion. Thermal, velocity and impurity boundary conditions are fully coupled between the Ar gas, Si feedstock and solid components of the system.

2. Modeling and Formulations

2.1 Global modeling strategies

The global simulation of coupled heat and mass transport in CZ-Si crystal growth involves three parts: (1) Computation of the thermal field of furnace components related to conduction and radiation; (2) Computation of the melting front, melt convection and impurity transport in the Si feedstock domain; (3) Computation of the Ar flow and species transport in the gas domain.[6)]

The configuration, dimensions and computational grids for the melting process of a CZ-Si crystal growth are shown in Fig. 1. The furnace was divided into a number of domains. The structured mesh was generated for solid and Si feedstock domains, while the unstructured mesh was used for the Ar gas domain. The interaction of impurities near the gas/melt interface is very critical in the CZ-Si growth process. Hence, the results at two locations in the gas (P_{Ar}) and the melt domain (P_{Si}) were monitored in the global simulations. The boundary information for velocity, temperature and impurities was exchanged at the interface between each component during the global simulation procedure. The algorithms for the global modeling of heat transfer have been published elsewhere.[10)]

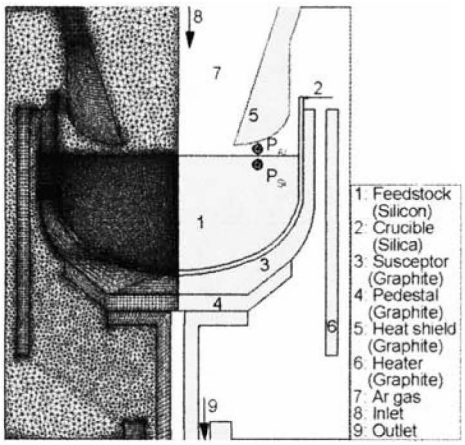

Fig 1. Geometry and mesh employed to simulate the melting process of CZ-Si crystal growth

2.2 Flow solvers for Ar gas and Si melt

The temperature difference in CZ-Si crystal growth is rather large, so the Boussinesq assumption is not applicable for analysis of Ar gas flow.[11)] In contrast, the velocity of Ar is relatively small. As a result, the compressibility of Ar gas is thermodynamically dominated. Therefore, the low Mach approximation and the ideal gas law were used in this simulation.[12)]

The enthalpy method for the convection/diffusion phase change problem on fixed grids[13)] was implemented to track the solid/liquid interface during the melting process. It was assumed that the Si feedstock domain was a continuum with fixed geometry. This assumption neglects the porosity and movement of block-shaped feedstock in the melting process. As well as the Boussinesq assumption, the Smagorinsky model[14)] was also introduced to describe the turbulent convection and transport in a large-diameter crucible. The velocity fields of the Si melt and Ar gas were computed simultaneously in a strictly coupled manner. The tangential velocity component and shear stress in both the Ar gas and Si melt were made equal to each other at the gas/melt interface.

2.3 Coupled model of O and C

The governing equations of O and C transport in the Si feedstock are written as follows:

$$\frac{\partial(\rho_{Si}c_O)}{\partial t}+\frac{\partial}{\partial x_i}(\rho_{Si}u_i c_O)=D_{eff}\frac{\partial^2 c_O}{\partial x_i^2}, \quad (1)$$

$$\frac{\partial(\rho_{Si}c_C)}{\partial t}+\frac{\partial}{\partial x_i}(\rho_{Si}u_i c_C)=D_{eff}\frac{\partial^2 c_C}{\partial x_i^2}, \quad (2)$$

where c_O and c_C are the molar concentration of O and C atoms, respectively. D_{eff} is the effective dynamic diffusivity of O and C atoms in the Si feedstock and is defined as follows:

$$D_{eff}=\mu/Sc+\mu_t/Sc_t. \quad (3)$$

Molecular and turbulent Schmidt numbers used were of 10 and 0.85, respectively [15)].

The governing equations for the transport of SiO and CO in the Ar gas are written as follows:

$$\frac{\partial(\rho_{Ar}\omega_{SiO})}{\partial t}+\frac{\partial}{\partial x_i}(\rho_{Ar}u_i\omega_{SiO})=D_{SiO}\frac{\partial^2(\rho_{Ar}\omega_{SiO})}{\partial x_i^2}, \quad (4)$$

$$\frac{\partial(\rho_{Ar}\omega_{CO})}{\partial t}+\frac{\partial}{\partial x_i}(\rho_{Ar}u_i\omega_{CO})=D_{CO}\frac{\partial^2(\rho_{Ar}\omega_{CO})}{\partial x_i^2}, \quad (5)$$

where ω_{SiO} and ω_{CO} are the mass fractions of SiO and CO in the mixed gas, respectively. D_{SiO} and D_{CO} are the diffusivity of SiO and CO, respectively, which are expressed as follows [5)]:

$$D_{SiO}=8.62611\times10^{-6}T^{1.75}/P_{Ar}, \quad (6)$$

$$D_{CO}=1.79548\times10^{-5}T^{1.75}/P_{Ar}. \quad (7)$$

The coupled boundary conditions for impurity transport were modeled based on the following reactions. The equations of the five considered reactions in a CZ-Si furnace are as follows:

(1)Crucible/susceptor corner

$$SiO_2(s)+C(s)\leftrightarrow CO(g)+SiO(g)$$

(2) Graphite fixture surfaces

$$SiO(g)+2C(s)\leftrightarrow CO(g)+SiC(s)$$

(3) Melt/crucible interface

$$SiO_2(s)\leftrightarrow Si(m)+2O(m)$$

(4) Gas/melt interface (for O)

$$Si(m)+O(m)\leftrightarrow SiO(g);$$

(5) Gas/melt interface (for C)

$CO(g) \leftrightarrow C(m) + O(m)$.

In the above equations, the index symbol (s) denotes solid, (m) denotes melt, and (g) denotes gas. A zero-flux boundary condition was used for C on the crucible wall. For non-C walls and the symmetry axis in gas, zero fluxes of SiO and CO were used; for the gas inlet, the concentrations of SiO and CO were set to zero; for the gas outlet, zero gradients of SiO and CO were used. These coupled boundary conditions have been described in our published papers.[7)]

3. Results and discussion

Transient global simulation was performed for the melting process of CZ-Si crystal growth. Thermal field, melt, and gas flow and impurity transport during growth were predicted with fully coupled boundary conditions of heat, flow, and impurities. The furnace pressure and Ar gas flow rate were set to 15 Torr and 10 SLPM, respectively. We defined three stages for the entire melting process. The first stage was when the melting front had not reached the top of the feedstock and the melt had not contacted the gas. The second stage was when the melting front had reached the top feedstock and the melt had contacted the gas. The third stage was when the melting process had finished and there was no solid feedstock.

3.1 Impurity transport before the melting front contacts Ar gas

The melting process of Si feedstock started from the lower side of the crucible. The distributions of SiO and CO in the gas domain are presented in Fig. 2(a) for one state in the first stage (time = 100 min). It was assumed that only reaction (1) was activated for SiO generation before the melting front contacted the gas. Gaseous SiO and CO were generated in the corner between the quartz crucible and the graphite susceptor by reaction (1). The maximum concentrations of SiO and CO were located around this corner. The resultant SiO was transported to the chamber where it reacted with the graphite components. Most of the SiO was absorbed, and CO was generated on the surface of the heated graphite components through reaction (2). The concentration of SiO was very low near the graphite surfaces. Then, gaseous CO was transported away by the gas flow.

In this stage, O was dissolved from the crucible wall through wetting by the melt. The corresponding concentration of O in the Si feedstock is presented on the left side of Fig. 2(b). Dissolved O accumulated in the melt domain without evaporation from the top surface. There was no contamination by C in this stage. The velocity vectors in the melted domain are shown on the right side of Fig. 2(b). An anticlockwise vortex was observed because of the buoyancy force. The first stage of the melting process was idealized to simplify the simulation. In a real system, the melting front could contact the Ar gas considerably earlier than in this simulation because of the block shape of the Si feedstock. Furthermore, evaporation of O and contamination with C may be initiated during the first stage.

3.2 Impurity transport after the melting front contacts Ar gas

The melting front reaches the top surface of the Si feedstock during the second stage of the melting process. Once the melt contacts the gas, reactions (4) and (5) can occur at the gas/melt interface. The distributions of SiO and CO in the gas domain are shown in Fig. 3(a) for one state in the second stage (time = 175 min). In this stage, O in the melt could evaporate promptly into the gas domain through reaction (4). A high concentration of gaseous SiO was found near the melt surface. Conversely, the increased concentration of SiO in the chamber promoted reaction (2). Thus, considerably more CO was generated along the graphite surfaces. The concentrations of SiO and CO in the gas domain were more than 10 times those in the first stage.

In this stage, the amount of O in the Si feedstock decreased dramatically because of SiO evaporation at the gas/melt interface. A large gradient of O concentration was observed near the melt surface, as can be seen on the left side of Fig. 3(b). Meanwhile, the resultant CO in the chamber diffused back to the free surface of the melt. The occurrence of reaction (5) resulted in contamination of the Si feedstock with C. The right side of Fig. 3(b) gives the corresponding distribution of C in the feedstock. The maximum concentration of C in the feedstock was located near the free surface of the melt, as was the maximum gradient of C concentration. Although the contamination with C was very low in this state, of the order of 10^{15} atoms/cm3, the incorporation of C accumulated during this transient process. Moreover, the concentration of C was homogenized by the convection in the melt during the melting process.

3.3 Accumulation of C in the final stage of the melting process

The melting process proceeded until all the Si feedstock melted. The concentrations of O, C, SiO, and CO equilibrated at the gas/melt interface after the melting process was complete. The distributions of SiO and CO in the gas domain of the third stage (time = 300 min) are presented in Fig. 4(a). The maximum concentrations of SiO and CO in the gas were both of the order of 10^{-8} mol/cm3. Evaporation of O and contamination with C at the gas/melt interface also reached equilibrium.

The final distributions of O and C in the melt are illustrated on the left and right sides of Fig. 4(b), respectively. A larger gradient of O concentration was observed near the gas/melt interface owing to the evaporation of SiO. Contamination of the melt with C increased by about one order compared with that in the second stage. This indicates

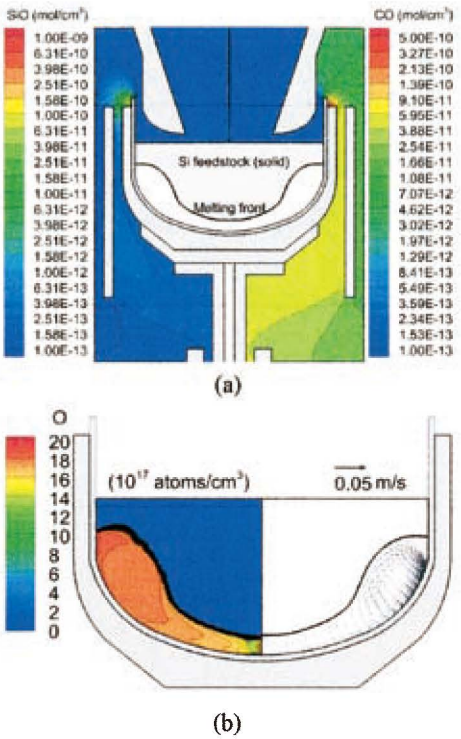

Fig. 2 Impurity transport during the first stage of the melting process: (a) Concentrations of SiO and CO in the Ar gas domain; (b) O concentration and melt flow in the Si feedstock.

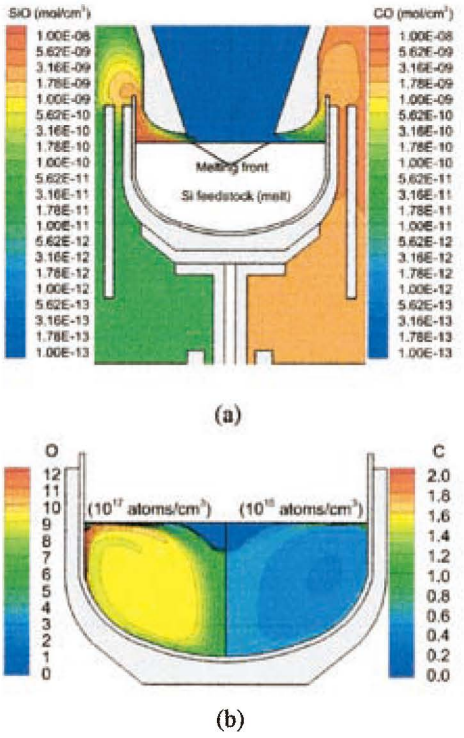

Fig. 3 Impurity transport during the second stage of the melting process: (a) Concentrations of SiO and CO in the Ar gas domain; (b) concentration of O and C in the melt.

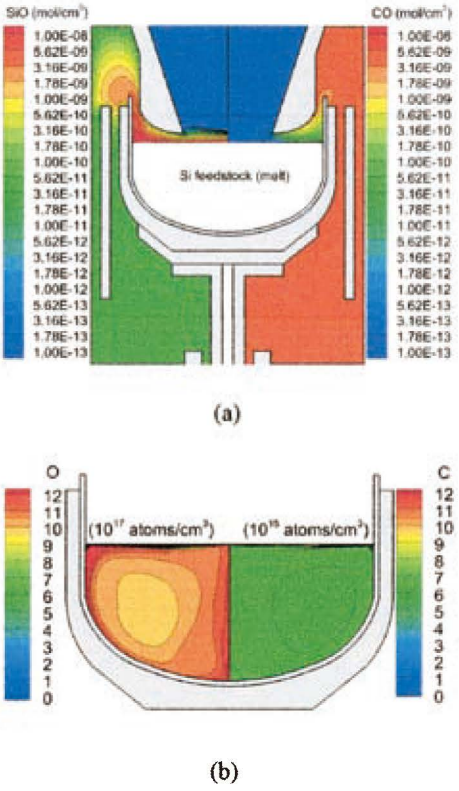

Fig. 4 Impurity transport during the third stage of the melting process: (a) Concentrations of SiO and CO in the Ar gas domain; (b) concentration of O and C in the melt.

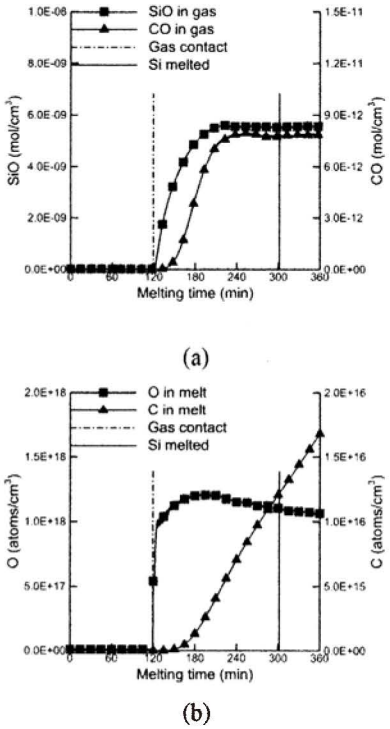

Fig. 5 Dynamic behavior of impurity transport during the melting process: (a) Concentrations of SiO and CO in the Ar gas domain; (b) Concentration of O and C in the melt.

the remarkable accumulation of C in the Si feedstock. This C could be incorporated into the crystal during the crystallization process. Therefore, control of contamination by C in the melting process is essential.

3.4 Dynamic behavior of O and C during the melting process

It is important to investigate the dynamic behavior of impurity generation and accumulation in the feedstock. To analyze the generation and accumulation of impurities, SiO and CO in the gas, O and C in Si feedstock were monitored for each time step. Figure 5(a) plots the concentrations of SiO and CO at the monitor point P_{Ar}. The critical state of C contamination is very noticeable. Once the melting front contacted with the Ar gas, both SiO and CO above the gas/melt interface increased rapidly, and then became stable. Figure 5(b) plots the concentrations of C and O in the feedstock at the monitor point P_{Si} during the melt process. The increase of CO activates C contamination from the gas/melt interface. In real CZ-Si crystal growth, the transition from the first to second stage should not be this steep because of the block shape of the feedstock. The evaporated SiO was carried by the gas to the chamber and reacted with the graphite components. The increase of CO resulted in the contamination increase from the melt free surface by C.

4. Conclusion

To investigate the generation and accumulation of impurities during CZ-Si crystal growth, a transient global simulation was performed with fully coupled boundary conditions of heat, flow and impurities. The melting process accompanied by C contamination of Si feedstock was predicted firstly by the introduction of the enthalpy method to overcome the convection/diffusion phase change problem. The dynamic behavior of O and C transport during the melting process was revealed. Contamination with C started once the melting front and Ar gas contacted. C accumulated in the melt until the end of the melting process. For accurate control of C concentration in crystals, the accumulation of C during the melting stage should be taken into account. Optimization of the melting process of the Si feedstock may be able to reduce the contamination of CZ-Si crystals by C.

Acknowledgment

This work was partially supported by the New Energy and Industrial Technology Development Organization (NEDO) under the Ministry of Economy, Trade and Industry (METI), Japan.

References

1) H. M. Liaw, Oxygen and carbon in Czochralski-grown silicon, Microelectr. J., 12, 33 (1981).

2) B. O. Kolbesen and A. Mühlbauer, Carbon in silicon: Properties and impact on devices, Solid State Electron, 25, 759 (1982).

3) M. S. Kulkarni, Defect dynamics in the presence of oxygen in growing Czochralski silicon crystals, J. Cryst. Growth, 303, 438 (2007).

4) L. Raabe, O. Pätzold, I. Kupka, J. Ehrig, S. Würzner and M. Stelter, The effect of graphite components and crucible coating on the behaviour of carbon and oxygen in multicrystalline silicon, J. Cryst. Growth, 318, 234 (2011).

5) D. E. Bornside, R. A. Brown, T. Fujiwara, H. Fujiwara and T. Kubo, The effects of gas-phase convection on carbon contamination of Czochralski-grown silicon, J. Electrochem. Soc., 142, 2790 (1995).

6) B. Gao and K. Kakimoto, Global simulation of coupled carbon and oxygen transport in a Czochralski furnace for silicon crystal growth, J. Cryst. Growth, 312, 2972 (2010).

7) B. Gao, S. Nakano and K. Kakimoto, Global simulation of coupled carbon and oxygen transport in a unidirectional solidification furnace for solar cells, J. Electrochem. Soc., 157, H153 (2010).

8) Z. Y. Li, L. J. Liu, W. C. Ma and K. Kakimoto, Effects of argon flow on impurities transport in a directional solidification furnace for silicon solar cells, J. Cryst. Growth, 318, 304 (2011).

9) A. N. Vorob'ev, A. P. Sid'ko and V. V. Kalaev, Advanced chemical model for analysis of Cz and DS Si-crystal growth, J. Cryst. Growth, 386, 226 (2014).

10) L. J. Liu and K. Kakimoto, Partly three-dimensional global modeling of a silicon Czochralski furnace. I. Principles, formulation and implementation of the model, Int. J. Heat Mass. Tran, 48, 4481 (2005).

11) R. Becker and M. Braack, Solution of a stationary benchmark problem for natural convection with large temperature difference, Int. J. Therm. Sci., 41, 428 (2002).

12) Z. Y. Li, L. J. Liu, W. C. Ma and K. Kakimoto, Effects of argon flow on heat transfer in a directional solidification process for silicon solar cells, J. Cryst. Growth, 318, 298 (2011).

13) V. R. Voller, M. Cross and N. C. Markatos, An enthalpy method for convection/diffusion phase change, Int. J. Numer. Meth. Eng, 24, 271 (1987).

14) J. Smagorinsky, General circulation experiments with the primitive equations, Mon. Weather. Rev., 91, 99 (1963).

15) A. D. Smirnov and V. V. Kalaev, Development of oxygen transport model in Czochralski growth of silicon crystals, J. Cryst. Growth, 310, 2970 (2008).